VIII International Conference on Particle-Based Methods
PARTICLES 2023
U. Perego, M. Cremonesi, A. Franci (Eds)

VERIFICATION OF A MESHLESS GENERALISED FINITE DIFFERENCE MIXING MODEL FOR FLUID-SOLID COUPLING

J. C. JOUBERT[1], D. N. WILKE[1] AND P. PIZETTE[2,3]

[1] Department of Mechanical and Aeronautical Engineering,
University of Pretoria,
South Africa

[2] IMT Nord Europe,
Institut Mines-Télécom,
Centre for Materials and Processes,
F-59000 Lille, France

[3] Univ. Lille,
Institut Mines-Télécom,
Univ. Artois, Junia,
ULR 4515 - LGCgE - Laboratoire de Génie Civil et géoEnvironnement,
F-59000 Lille, France

Abstract: This work extends a multi-phase mixing model framework designed for a Smoothed Particle Hydrodynamics context. Specifically, we propose a higher-order variation using the first-order accurate Generalised Finite Difference differential operators to construct an incompressible scheme for simulating fluid-solid coupled systems resolved via a continuum mixture model. The proposed scheme incorporates inter-phase shear between phases and the viscosity dependency of the solid phase concentration. The scheme is verified by simulating a modified lid-driven cavity case at $Re = 1000$. In this simulation, our method was capable of treating initially discontinuous concentration fields with a maximum solid volume concentration of 0.5 and a solid-to-fluid density ratio of 4.

Keywords. Generalised Finite Difference (GFD), Meshless Lagrangian Method (MLM), Concentration Model, Multiphase, Multiphysics

1 INTRODUCTION

The interaction between granular and fluid media is of significant interest due to its abundance in physical and engineering processes. Particle-laden flow is one phenomenon in this class that refers to fluid flow in which solid particles are suspended and transported by the fluid. The interest in simulating particle-laden flow is driven by its central role in processes such as erosion, waste transport, pollution management and process engineering systems such as pneumatic transport and fluidised bed reactors.

As this is an inherently multi-physics phenomenon, appropriate treatment typically is computationally expensive. However, with the rising popularity of massively paral-

lelisable schemes such as the discrete element method (DEM) and meshless Lagrangian methods (MLMs) as well as the rapid adoption of general-purpose GPUs as computational hardware, these systems have become tractable to solve at an increased fidelity.

At the granular particle level, the interaction between media can be treated as a fully coupled fluid-solid interaction (FSI) problem [1, 2, 3]. Although this approach is conceptually valid at any scale, from a practical standpoint, this rapidly becomes intractable as the number of granular particles increases. Approaches have been developed to address this by simplifying the fluid-granular interaction and solid phase representation so that the system is tractable to resolve. Due to the inherently multi-scale and multi-physics nature of these systems, various models have been proposed such that the dominant physics is treated appropriately. As an example, mesoscale coupling [4, 5, 6] is appropriate for systems where granular particles can be resolved individually, but the coupling forces must be resolved via empirical correlations. In contrast, mixture models are employed when the number of granular particles is so large that it is not tractable to resolve individual granular particles. Rather the granular medium is represented by a dynamic field that interacts with a fluid phase in a volume-averaged sense [7, 8, 9, 10, 11].

First introduced in an MLM context to treat solid phases as a continuum, the multi-phase formulation of [7] was adopted in the weakly compressible smoothed particle hydrodynamics (SPH) formulation of Ren et al. [8]. This work extends each SPH particle to include concentration and diffusion velocity parameters while the particles are advected according to the mean-field velocity. The concentration parameter resolves the composition of each phase represented by the particle. The diffusion velocity specifies the velocity difference between the phase and the mean-field velocity. This introduces the idea of intrinsic shear between phases, resulting in an additional shear term in the mean-field momentum conservation equations. This formulation was later extended by Yan et al. [9] to incorporate solid phase constitutive models into the weakly compressible SPH solver. This allowed for the simulation of a dry solid phase interacting with the fluid phase while being able to resolve dissolution.

As with other under-resolved models, closure is achieved through an empirical model. For the mixture model, the closure relationship resolves the diffusion velocity, which is used to construct its shear contribution. In [11], Jiang et al. introduced a closure model that identically enforces mass conservation by ensuring the appropriate divergence-free condition of the diffusion velocities. Furthermore, the particle velocity was set to the volumetric flux rather than the mean-field velocity. This implies that the particle flow velocity is divergence-free allowing typical incompressible MLM techniques to be applied with little modification.

The choice to use classic SPH operators in computer graphics is sensible due to their relatively inexpensive computational cost. However, accuracy is often more desirable than speed in a scientific and engineering context. Kernel renormalisation [12, 13] is a modification that raises the order of SPH operators from zeroth- to first-order accurate. As a trade-off for the increased accuracy, this significantly increases the computational cost. Alternatively, the generalised finite difference (GFD) method [14, 15, 16] makes use of first-order accurate operators that result in similar behaviour to renormalised SPH

while being more computationally efficient [17].

To make progress toward a meshless mixture model formulation for engineering contexts, this paper proposes an incompressible GFD-based scheme based on the mathematical model described in [11]. The scheme is verified by simulating a lid-driven cavity at $Re = 1000$ and comparing the results against finite volume method (FVM) and SPH results. Furthermore, the evolution of the concentration field is presented and quantified, allowing for comparison with other mixing models and schemes.

2 MATHEMATICAL MODEL

Like other MLMs, the GFD method operates by dynamically building a neighbour list of local particles that it then uses to construct the appropriate differential operators. The discretised partial differential equations (PDEs) are constructed at a particle level from these differential operators. Since the PDEs are cast in a Lagrangian frame, advection is directly treated by updating the particle positions. At the same time, the evolution of the material state is resolved from the evolution equations. In this work, the solid phase is incorporated by assigning each particle with a solid volume concentration, indicating the composition of the continuum at the particle location. As such, in addition to the mean-field Navier-Stokes equations (NSE), an evolution equation for the solid concentration must also be solved.

The notion adopted in this work makes use of bold characters to indicate tensors. Bold lowercase Latin symbols are use to indicate rank-1 tensors while bold Greek and uppercase Latin symbols are used to indicate rank-2 tensors. Inner products are indicated by $(\bullet)\cdot(\bullet)$ while outer products are indicated by $(\bullet)\otimes(\bullet)$.

This work uses the MLM framework proposed in [11], where SPH was used to discretise the mixing model. When considering each phase as an incompressible material, the mass conservation of each phase can be written as:

$$\partial_t \alpha_k + \nabla \cdot (\alpha_k \mathbf{u}_k) = 0, \tag{1}$$

where α_k is the concentration, $\mathbf{u}_k$ is the velocity and $k \in \{s, f\}$ is a subscript used to indicate either the solid or the fluid phase, respectively. By adding the fluid and solid mass conservation equations and considering $\alpha_s + \alpha_f = 1$, the mean-phase mass conservation can be written as:

$$\nabla \cdot \mathbf{u}_m = 0, \tag{2}$$

where $\mathbf{u}_m = \sum_k (\alpha_k \mathbf{u}_k)$. It should be mentioned that this is not the mean-phase velocity as described in [7], but rather the volumetric flux.

As motivated in [11], the reason for choosing the volumetric flux over the mean-phase velocity is due to the divergence-free condition allowing for a single-phase incompressible solver to be applied to this system. From a numerical perspective, the divergence-free condition also suggests that particles are less inclined to separate or cluster when flowing between dilute and dense solid clusters. However, clustering due to converging streamlines must still be addressed. For this, the anti-clustering algorithm of Xu et al. [18]

is employed. With the volumetric flux being used as the particle velocity, the material derivative is now defined as $D_t = \partial_t + \mathbf{u}_m \cdot \nabla$.

Since α_f can be fully described by α_s, only the solid phase concentration is explicitly tracked. Writing (1) for the solid phase in terms of the volumetric flux:

$$D_t \alpha_s = -\nabla \cdot (\alpha_s \mathbf{u}_{ms}), \tag{3}$$

introduces the diffusion velocity $\mathbf{u}_{ms} = \mathbf{u}_s - \mathbf{u}_m$.

Similarly, the mean-phase momentum conservation equation is constructed by adding the volume-averaged equations of motion of each phase:

$$D_t \mathbf{u}_m = -\gamma \nabla p_m + \frac{1}{\rho_m} \nabla \cdot \boldsymbol{\tau}_m + \nabla \cdot \left(\frac{\boldsymbol{\tau}_d}{\rho_m} \right) + \mathbf{g}, \tag{4}$$

where p_m is the mean-field pressure, $\boldsymbol{\tau}_m$ is the mean-field shear stress, $\boldsymbol{\tau}_d$ is the inter-phase shear stress, $\mathbf{g}$ is the body force and $\gamma = \sum_k \alpha_k / \rho_k$ with ρ_k the phase density.

The volumetric flux is used to resolve the mean-field shear stress as:

$$\boldsymbol{\tau}_m = \mu_m \left[(\nabla \otimes \mathbf{u}_m) + (\nabla \otimes \mathbf{u}_m)^T \right], \tag{5}$$

where μ_m is the mean-phase dynamic viscosity resolved as a function of the fluid viscosity μ_f and the solid concentration:

$$\mu = \mu_f \left(1 - \frac{\alpha_s}{\alpha_{sm}} \right)^{-2{,}5\alpha_{sm}}, \tag{6}$$

where $\alpha_{sm} \approx 0.62$ is the concentration at the maximum solid packing [7].

The inter-phase shear stress arises due to the difference between the velocities of individual phases and the volumetric flux. It so is completely determined by the diffusion velocity and concentration:

$$\boldsymbol{\tau}_d = -\rho_m \sum_k \alpha_k \mathbf{u}_{mk} \otimes \mathbf{u}_{mk}. \tag{7}$$

2.1 GFD discretisation

The GFD operators [14, 15, 16] are a class of meshless operators that allow differential operators to be approximated from discrete field values obtained from an unstructured point cloud. While they take on a similar form to kernel renormalised SPH, these operators do not rely on kernel gradient directly. Rather, they opt to weight finite difference terms with a kernel function. This makes the operators more computationally efficient when compared to renormalised SPH schemes while producing similar behaviour [17].

This work makes use of a quintic kernel [19]:

$$W(\mathbf{r}, h) = \begin{cases} (3-q)^5 - 6(2-q)^5 + 15(1-q)^5 & \text{for } 0 \leq q \leq 1 \\ (3-q)^5 - 6(2-q)^5 & \text{for } 1 < q \leq 2 \\ (3-q)^5 & \text{for } 2 < q \leq 3 \\ 0 & \text{otherwise} \end{cases} \quad \text{with} \quad q = \|\mathbf{r}\|/h, \tag{8}$$

where $3h$ is the support radius of the kernel.

For the sake of readability, the relative distance between two particles is written as $\mathbf{r}_{ij} = \mathbf{r}_i - \mathbf{r}_j$. This extends to the evaluation of the kernel function between two particles where the notation $W_{ij} = W(\mathbf{r}_{ij}, h)$ is adopted. Similarly, the notation $f_i = f(\mathbf{r}_i)$ will be adopted for any field value at a particle location.

For a generalised field f, the GFD gradient can be written as:

$$\langle \nabla f \rangle_i = \mathbf{B}_i \cdot \sum_j (f_i - f_j) W_{ij} \mathbf{r}_{ij}, \tag{9}$$

with:

$$\mathbf{B}_i^{-1} = \sum_j W_{ij} \mathbf{r}_{ij} \otimes \mathbf{r}_{ij}, \tag{10}$$

The GFD Laplacian operator can be written as:

$$\left\langle \nabla^2 f \right\rangle_i = 2dL_i \sum_j (f_i - f_j) W_{ij} (1 - \mathbf{r}_{ij} \cdot \mathbf{o}_i), \tag{11}$$

where d is the system dimension, $\mathbf{o}_i$ the renormalised offset vector:

$$\mathbf{o}_i = \mathbf{B}_i \cdot \sum_j W_{ij} \mathbf{r}_{ij}, \tag{12}$$

and L_i is the normalisation factor:

$$L_i^{-1} = \sum_j \|\mathbf{r}_{ij}\|^2 W_{ij} (1 - \mathbf{r}_{ij} \cdot \mathbf{o}_i), \tag{13}$$

with $\|(\bullet)\|$ indicating the Euclidean norm.

Due to the large density difference possible between particles, the pressure term is resolved with density smoothing. Specifically, the pressure term is resolved as:

$$\langle \gamma \nabla p_m \rangle_i = \mathbf{B}_i \cdot \sum_j \frac{2\gamma_i \gamma_j}{\gamma_i + \gamma_j} (p_{m,i} - p_{m,j}) W_{ij} \mathbf{r}_{ij}, \tag{14}$$

Furthermore, the mean-phase shear term is resolved by splitting the differential operator:

$$\langle \nabla \cdot \boldsymbol{\tau}_m \rangle_i = \mu_i \left\langle \nabla^2 \mathbf{u}_m \right\rangle + \left. \frac{d\mu_i}{d\alpha_s} \right|_{\alpha_{s,i}} \langle \nabla \alpha_s \rangle_i \cdot \left(\langle \nabla \otimes \mathbf{u}_m \rangle_i + \langle \nabla \otimes \mathbf{u}_m \rangle_i^T \right), \tag{15}$$

where $d\mu_i / d\alpha_s$ is analytically determined from (6).

2.2 Concentration model

To close the system, the diffusion velocity $\mathbf{u}_{mk}$ must be resolved. The closure model of [11] is adopted in this work along with their evolution scheme for the solid phase concentration.

To resolve the drift velocity, it is decomposed into two components $\mathbf{u}_{mk} = \mathbf{u}^0_{mk} + \mathbf{u}^1_{mk}$ with $\mathbf{u}^0_{mk}$ modelling the relative advection of the phase while $\mathbf{u}^1_{mk}$ resolves the diffusion of the phase.

These components are resolved as:

$$\mathbf{u}^0_{mk} = C^0_m \frac{\rho_k - \rho_m}{\rho_m}(\mathbf{g} - D_t \mathbf{u}_m), \tag{16}$$

$$\mathbf{u}^1_{mk} = -\frac{C^1_m}{\alpha_k}\nabla \alpha_k, \tag{17}$$

where C^0_m and C^1_m are parameters that control the advection and diffusion effects. As specified in [11], these parameters should be in the range of 0.001 to 0.01. In this work, we use $C^0_m = 0.002$ and $C^1_m = 0.001$.

With this approach, (3) can now be written as:

$$D_t \alpha_s = -\nabla \cdot (\alpha_s \mathbf{u}^0_{ms}) + C^1_m \nabla^2 \alpha_s. \tag{18}$$

To avoid undefined cases, $\mathbf{u}_{mk} = 0$ when $\alpha_k = 0$. However, even in these cases, the evolution equation is always valid regardless of the solid concentration.

The diffusion component is discretised using the standard GFD Laplacian $C^1_m \langle \nabla^2 \alpha_s \rangle$ while the advection component is resolved directly as:

$$\left\langle \nabla \cdot (\alpha_s \mathbf{u}^0_{ms}) \right\rangle_i = \sum_j W_{ij}(\alpha_{s,i}\mathbf{u}^0_{ms,i} - \alpha_{s,j}\mathbf{u}^0_{ms,j}) \cdot \mathbf{B}_i \cdot \mathbf{r}_{ij}. \tag{19}$$

It should be noted that the particle acceleration from the previous step is used to determine the current $\mathbf{u}^0_{ms}$.

2.3 Pressure Poisson equation

The incompressibility condition is implicitly enforced through a prediction-projection scheme like that first proposed in the context of SPH by Xu et al. [18].

For iteration k, a predictor step maps the velocity field $\mathbf{u}^k_{m,i}$ to an intermediate state $\mathbf{u}^*_{m,i}$ by incorporating all acceleration terms except for those due to the pressure gradient:

$$\mathbf{u}^*_{m,i} = \mathbf{u}^k_{m,i} + \Delta t \left(\frac{\left\langle \nabla \cdot \boldsymbol{\tau}^k_m \right\rangle_i}{\rho^k_{m,i}} + \left\langle \nabla \cdot \left(\frac{\boldsymbol{\tau}_d}{\rho_{m,i}} \right)^k \right\rangle_i + \mathbf{g}_i \right), \tag{20}$$

where Δt is the time-step size.

Using this intermediate velocity, the pressure field is obtained by solving the pressure Poisson equation (PPE) constrained such that the resulting pressure gradient suppresses the divergence of the intermediate velocity field:

$$\left\langle \nabla \cdot (\gamma^k \nabla p^{k+1}_m) \right\rangle_i = \frac{1}{\Delta t} \left\langle \nabla \cdot \mathbf{u}^*_m \right\rangle_i \tag{21}$$

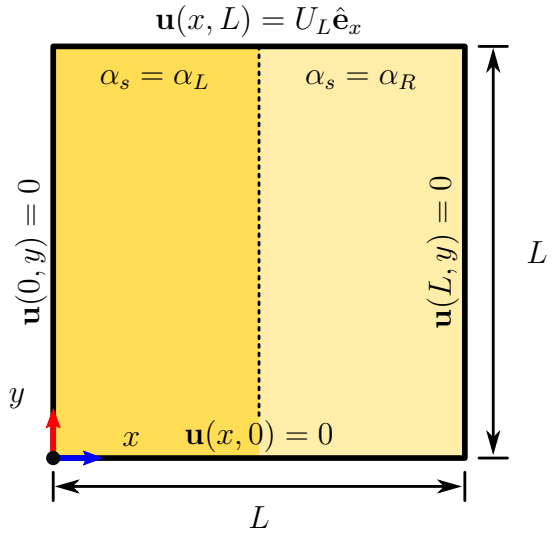

Figure 1: Schematic description of the initial and boundary conditions of the lid-driven cavity case.

with:

$$\left\langle \nabla \cdot (\gamma^k \nabla p_m) \right\rangle_i = 2dL_i \sum_j \frac{2\gamma_i\gamma_j}{\gamma_i + \gamma_j}(p_{m,i} - p_{m,j})W_{ij}(1 - \mathbf{r}_{ij} \cdot \mathbf{o}_i). \tag{22}$$

This results in an $n \times n$ sparsely coupling linear system that must be solved to recover the particle pressures. The system is solved using a bi-conjugate gradient stabilised (BiCGSTAB) linear solver with a Jacobi preconditioner. For a detailed description of the PPE solver, the reader is directed to [20].

3 RESULTS

The lid-driven cavity problem is explored in this work for verification of the solver. The system is tuned such that the fully mixed state corresponds to the single-phase case at $Re = 1000$ where $Re = U_L L/\nu_m$ is the Reynolds number, L is the cavity length, U_L is the lid velocity and $\nu_m = \mu_m/\rho_m$ is the kinematic viscosity. A schematic description of the system can be seen in Figure 1 with $L = 1\text{m}$ and $U_L = 1\text{m/s}$. The initial solid volume concentration is set to $\alpha_L = 0.0$ and $\alpha_R = 0.5$ for the left and right domains, respectively. An initial particle spacing of 0.05m is used.

The fully mixed state should correspond to the concentration averaged over the domain $\alpha_{\text{mix}} = (\alpha_L + \alpha_R)/2$. The material properties are based on this steady-state solution such that $\nu_m(\alpha_{\text{mix}}) = 1 \times 10^{-3}\text{m}^2/\text{s}$. The material properties can be seen in Table 1.

The results are organised into two sections. The first section investigates the behaviour of the concentration field. Analysing the evolution of the concentration field distribution provides context for how the the mixing model affect the material properties of the system. Furthermore, this allows the assumption of a uniform solid volume concentration at steady-state to be verified while also quantifying the error of this assumption.

Table 1: Material properties for the lid-driven cavity case.

Property	Symbol	Value	
Fluid density	ρ_f	1.0	kg/m^3
Solid density	ρ_s	4.0	kg/m^3
Fluid viscosity	μ_f	7.862×10^{-4}	Pa·s

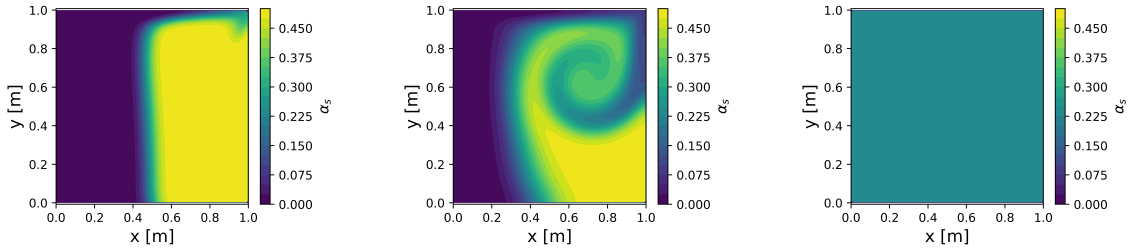

(a) (b) (c)

Figure 2: 2D concentration field snapshots at time (a) 1.0s, (b) 5.0s and (c) 100.0s.

The final section investigates the evolution and steady state response of the velocity field. The evolution of the velocity field provides insight into how the mixing model affects the behaviour of the continuum while the steady state response is compared against other numerical results for verification of the scheme in a uniform concentration configuration.

3.1 Concentration evolution

The evolution of the concentration field is shown in Figure 2. This shows that the initial evolution is strongly dictated by the advection of the fluid particles, which results in the spiralling structure forming along the fluid streamlines. Diffusion is also most active during this time due to the concentration gradients being largest at the start of the simulation.

Figure 3 shows the corresponding kinematic viscosity field evolution. As a single parameter model, the viscosity directly correlates to the concentration field, albeit through

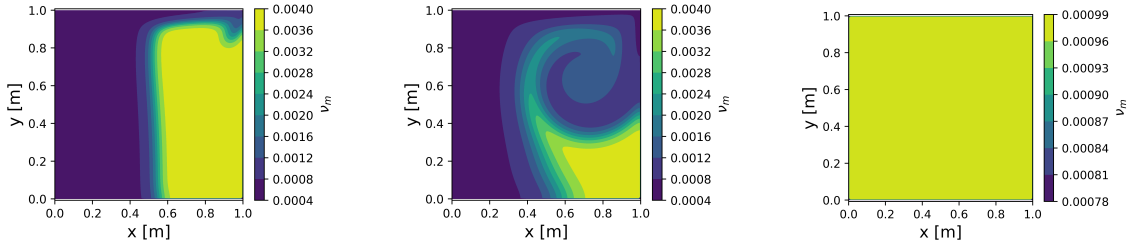

(a) (b) (c)

Figure 3: 2D kinematic viscosity field snapshots at time (a) 1.0s, (b) 5.0s and (c) 100.0s.

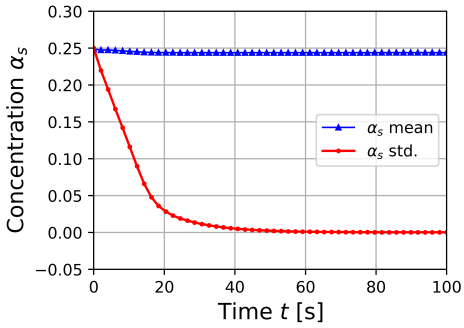

Figure 4: Evolution of the solid phase concentration mean and standard deviation.

a power law scaling that serves to suppress its effects in lower concentration regions.

As advection mixes particles of dissimilar regions and diffusion smooths out local differences, the concentration tends towards a uniform state. This is quantified in Figure 4, where the evolution of the average particle concentration and standard deviation is shown. As expected from a mass conservation argument, the average concentration is nearly constant, with an initial average concentration of 0.249 compared to a final value of 0.244.

When considering the standard deviation trends, it can be noticed that the concentration evolution has two regimes. Between 0.0s and 20.0s, the standard deviation undergoes linear decay. During this time, the mixing of the two regions is the primary driver. From 20.0s to 100.0s, the decay rate is noticeably slower as most of the fluid is well mixed. Here, diffusion is the primary driver for concentration evolution. After 100.0s a standard deviation of 0.1% relative to the average concentration was obtained. As such, the steady-state quasi-static behaviour of the concentration field is well approximated by the final simulation state.

3.2 Velocity field evolution

The velocity field snapshots corresponding to the concentration field snapshots can be seen in Figure 5. The increased mass and viscosity of the high-concentration region results in high flow resistance as can be seen by the evolution of the velocity field at the beginning of the simulation where the boundary layer development is noticeably thicker in the high-concentration region.

The mid-plane velocities are shown in Figure 6. As mentioned above, with the concentration tending towards a uniform distribution, the steady-state results are expected to match the classic lid-driven cavity case with $Re = 1000$. As such, the results at 100.0s are compared against the FVM results of Ghia et al. [21] and the incompressible SPH results of Xu et al. [18]. Although all results agree generally, the current results are noticeably more similar to the FVM results, especially at the extreme values. When compared against the FVM results, a maximum difference of 2.2% relative to the velocity range was found. The discrepancy is partially due to the solid concentration having a true value of 0.244 rather than the estimated 0.25 used to set the fluid material properties.

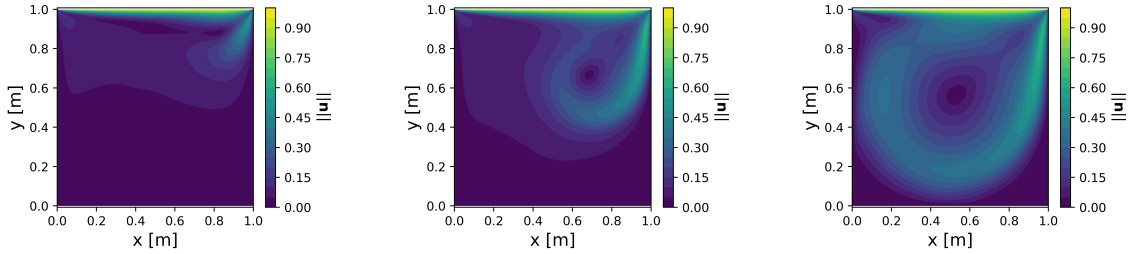

(a) (b) (c)

Figure 5: 2D velocity magnitude field snapshots at time (a) 1.0s, (b) 5.0s and (c) 100.0s.

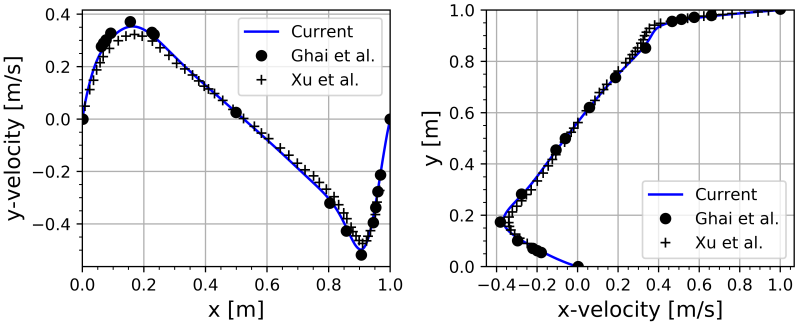

Figure 6: Steady-state mid-plane velocity results for the lid-driven cavity at $Re = 1000$.

4 CONCLUSIONS

This work describes a renormalised meshless scheme for simulating fluid-solid mixing resolved at the continuum scale using GFD operators. The scheme was applied to the classic lid-driven cavity problem, which was modified to incorporate multi-species flow. The solid volume concentration field was initialised with a step discontinuity.

It was found that the concentration distribution decayed in a two-regime process. The first regime was driven primarily by the mixing of the continuum, while the second was primarily driven by diffusion. The combined effect resulted in uniform concentration distribution at the final simulation time. The final average concentration of 0.244 was compared to the expected concentration of 0.249, showing a 2.0% violation in the solid phase mass conservation.

The velocity field was shown to be affected by the concentration field, with its evolution responding to the increased flow resistance resulting from an increased density and viscosity. Even so, as the simulation progressed towards steady-state, the results converged to those of the classic lid-driven cavity case with a maximum error of 2.2% when compared against FVM results.

Opportunities for further verification and validation studies are present, especially for free surface cases. Furthermore, the development of calibration techniques for the numerical advection and diffusion parameters must be established. Finally, multi-physics coupling with other fluid-solid schemes such as fully- and under-resolved GFD-DEM can

also be explored to create multi-fidelity fluid-granular coupling schemes.

REFERENCES

[1] Hashemi, M.R., Fatehi, R., and Manzari, M.T. A modified SPH method for simulating motion of rigid bodies in Newtonian fluid flows. *International Journal of Non-Linear Mechanics* (2012) **47(6)**:626-638.

[2] Joubert, J.C., Wilke, D.N., Govender, N., Pizette, P., Tuzun, U. and Abriak, N.E. 3D gradient corrected SPH for fully resolved particle–fluid interactions. *Applied Mathematical Modelling* (2020) **78**:816-840.

[3] Peng, C., Zhan, L., Wu, W., and Zhang, B. A fully resolved SPH-DEM method for heterogeneous suspensions with arbitrary particle shape. *Powder Technology* (2021) **387**:509-526.

[4] Fernandez, J.W., Cleary, P.W., Sinnott, M.D., and Morrison, R.D. Using SPH one-way coupled to DEM to model wet industrial banana screens. *Minerals Engineering* (2011) **24(8)**:741-753.

[5] Sun, X., Sakai, M., and Yamada, Y. Three-dimensional simulation of a solid–liquid flow by the DEM–SPH method. *Journal of Computational Physics* (2013) **248**:147-176.

[6] Robinson, M., Ramaioli, M., and Luding, S. Fluid–particle flow simulations using two-way-coupled mesoscale SPH–DEM and validation. *International journal of multiphase flow* (2014) **59**:121-134.

[7] Manninen, M., Taivassalo, V., and Kallio, S. On the mixture model for multiphase flow. (1996).

[8] Ren, B., Li, C., Yan, X., Lin, M.C., Bonet, J. and Hu, S.M., Multiple-fluid SPH simulation using a mixture model. *ACM Transactions on Graphics (TOG)* (2014) **33(5)**:1-11.

[9] Yan, X., Jiang, Y.T., Li, C.F., Martin, R.R., and Hu, S.M. Multiphase SPH simulation for interactive fluids and solids. *ACM Transactions on Graphics (TOG)* (2016) **35(4)**:1-11.

[10] Bui, H.H., and Nguyen, G.D. A coupled fluid-solid SPH approach to modelling flow through deformable porous media. *International Journal of Solids and Structures* (2017) **125**:244-264.

[11] Jiang, Y., Li, C., Deng, S. and Hu, S.M. A Divergence-free Mixture Model for Multiphase Fluids. *Computer Graphics Forum* (2020) **39**:69-77.

[12] Randles, P.W., and Libersky, L.D. Smoothed particle hydrodynamics: some recent improvements and applications. *Computer methods in applied mechanics and engineering* (1996) **139(1-4)**:375-408.

[13] Bonet, J., and Lok, T.S. Variational and momentum preservation aspects of smooth particle hydrodynamic formulations. *Computer Methods in applied mechanics and engineering* (1999) **180(1-2)**:97-115.

[14] Lanson, N. and Vila, J.P. Renormalized meshfree schemes I: consistency, stability, and hybrid methods for conservation laws. *SIAM Journal on Numerical Analysis* (2008) **46(4)**:1912-1934.

[15] Lanson, N. and Vila, J.P. Renormalized meshfree schemes II: convergence for scalar conservation laws. *SIAM Journal on Numerical Analysis* (2008) **46(4)**:1935-1964.

[16] Basic, J., Degiuli, N., and Ban, D.A class of renormalised meshless Laplacians for boundary value problems. *Journal of Computational Physics* (2018) **354**:269-287.

[17] Joubert, J.C., Wilke, D.N., Govender, N., Pizette, P., Basic, J., and Abriak, N.E. Boundary condition enforcement for renormalised weakly compressible meshless Lagrangian methods. *Engineering Analysis with Boundary Elements* (2021) **130**:332-351.

[18] Xu, R., Stansby, P., and Laurence, D. Accuracy and stability in incompressible SPH (ISPH) based on the projection method and a new approach. *Journal of Computational Physics* (2009) **228(18)**:6703-6725.

[19] Morris, J.P., Fox, P.J., and Zhu, Y. Modeling low Reynolds number incompressible flows using SPH. *Journal of computational physics* (1997) **136(1)**:214-226.

[20] Joubert, J.C., Wilke, D.N., and Pizette, P. A Generalized Finite Difference Scheme for Multiphase Flow. *Mathematical and Computational Applications* (2023) **28(2)**:51.

[21] Ghia, U.K.N.G., Ghia, K.N., and Shin, C.T. High-Re solutions for incompressible flow using the Navier-Stokes equations and a multigrid method. *Journal of computational physics* (1982) **48(3)**:387-411.